Drug Design, Development and Therapy

Dovepress
Taylor & Francis Group

Open Access Full Text Article

ORIGINAL RESEARCH

Oxysophocarpine Inhibits Apoptosis of Lung Epithelial Cells to Alleviate Acute Lung Injury via KIT/PI3K Signaling Pathway

Ziyao Qiao[1,*], Kaihua Long[1,2,*], Kairu Ding[1], Xiaoyan Zhang[2], Xiaoli Gao[1], Shanrong Han[1], Na Zheng[1], Yun Yang[1], Jingjing Li[1], Yaqiong Su[1], Hong Zhang[1,2], Ye Li[1,2], Wenbing Zhi[2], Yang Liu[1,2]

[1]College of Life Sciences, Northwest University, Xi'an, People's Republic of China; [2]Shaanxi Academy of Traditional Chinese Medicine (Shaanxi Traditional Chinese Medicine Hospital), Xi'an, People's Republic of China

*These authors contributed equally to this work

Correspondence: Yang Liu; Wenbing Zhi, Shaanxi Academy of Traditional Chinese Medicine (Shaanxi Traditional Chinese Medicine Hospital), No. 421 Zhuque Street, Xi'an, Shaanxi, 710061, People's Republic of China, Tel +86 02985395659, Email liuyang3111111@163.com; zhiwenbing@163.com

Purpose: Acute lung injury (ALI) is an acute, diffuse, inflammatory lung injury caused by many factors. Oxysophocarpine (OSC), a quinoline alkaloid sourced from traditional Chinese herbs *Sophora flavescens* and *Sophora davidii*, possesses anti-inflammatory and antioxidant properties. However, its effects on ALI are still unclear. This study aims to investigate the role and potential mechanisms of OSC for the treatment of ALI.

Methods: The levels of TNF-α, IL-6, and IL-1β in bronchoalveolar lavage fluid (BALF) were measured with an enzyme-linked immunosorbent assay (ELISA). Lung tissue changes were examined through hematoxylin and eosin (HE) staining. Lung cell apoptosis was analyzed using the terminal deoxynucleotidyl transferase dUTP nick-end labeling (TUNEL) assay. Flow cytometry was utilized to detect neutrophil aggregation. Further, the network pharmacology and molecular docking was employed to predict the mechanisms. Key pathways and targets of OSC were confirmed using methods like immunohistochemistry (IHC), immunofluorescence (IF), real-time quantitative PCR (RT-qPCR), and Western blotting (WB).

Results: In vivo, OSC treatment significantly inhibited diffuse alveolar injury and interstitial edema compared to the LPS-induced model mice, reduced neutrophil infiltration, and lowered lung epithelial cell apoptosis. In vitro, OSC pretreatment enhanced lung epithelial cell viability and decreased LPS-induced apoptosis. Network pharmacology analysis suggested that OSC mainly targeted key proteins in the PI3K/AKT and apoptosis signaling pathways, such as KIT, PIK3CA, and Bcl-2. Molecular docking confirmed that OSC binds strongly to these targets. Further, PCR, WB, IF, and IHC assay demonstrated that OSC pretreatment elevated PI3K, KIT, and Bcl-2 expressions in BEAS-2B lung epithelial cells and lung tissues.

Conclusion: OSC reduced inflammatory cytokine production, neutrophil aggregation, and lung epithelial cell apoptosis via regulating the KIT/PI3K signaling pathway.

Keywords: pharmacological, inflammation, acute lung injury, KIT/PI3K signaling pathway, immunity

Introduction

Acute lung injury (ALI) is a systemic inflammatory response triggered by various factors, including severe infection, trauma, shock, and burns.[1] It features inflammatory cell infiltration, increased vascular permeability, and diffuse interstitial and alveolar edema, causing acute respiratory failure.[2,3] Radiological examinations show heterogeneous exudative lesions in the lungs.[4] The US ALI incidence is 86.2 cases per 100,000 people, with a 38.5% mortality rate.[5] Furthermore, ALI often leads to acute respiratory distress syndrome (ARDS), with a 40% mortality rate.[6] In clinical practice, treatment for ALI generally involves the use of anti-inflammatory drugs and respiratory support measures, such as corticosteroids,[7] neutrophil elastase inhibitors, statins, and mechanical ventilation.[7–10] However, these treatment

Received: 3 June 2025
Accepted: 11 September 2025
Published: 23 September 2025

methods have limited effectiveness in reducing the mortality rate of ALI. Hence, exploring new ALI drugs and targets is crucial.

ALI is characterized by several pathological features and mechanisms, including inflammatory response, oxidative stress, alveolar-capillary barrier disruption, cell apoptosis, and tissue fibrosis. It progresses through exudation, proliferation, and fibrosis phases. The exudation phase is characterized by immune cell-mediated damage to the alveolar epithelium and the endothelial barrier. This damage results in the buildup of protein-rich edema and leukocytes in the interstitium and alveoli. Activated macrophages release inflammatory cytokines and apoptosis-inducing molecules, further worsening lung injury. A significant accumulation of neutrophils occurs in the lungs during the exudation phase, leading to the release of various inflammatory mediators and cytokines, including TNF-α, IL-1β, and IL-6.[11] Lipopolysaccharide (LPS), a major component of Gram-negative bacteria, is frequently used to create ALI models.[12] After LPS binds to LPS-binding protein (LBP) and the CD14 receptor, it is presented to Toll-like receptor 4 (TLR4). This triggers the activation of NF-κB, which initiates downstream signaling and leads to the activation of PI3K, regulating the release of inflammatory mediators like TNF-α, IL-1β, and IL-6.[13–16] Previous studies have shown that LPS-induced ALI in mice results in elevated levels of TNF-α, IL-1β, and IL-6 in BALF. The excess production of these cytokines activates and recruits neutrophils, exacerbating pulmonary inflammation.[17,18] Therefore, reducing the release of inflammatory mediators and neutrophil aggregation is vital for alleviating the onset and progression of ALI.

Acute Respiratory Distress Syndrome (ARDS), first formally described in 1967, evolves from ALI through a complex pathological cascade. The 2012 Berlin Definition refined diagnostic criteria by classifying ARDS into three severity tiers based on hypoxemia under positive end-expiratory pressure (PEEP ≥5 cm H_2O): mild (PaO_2/FiO_2 = 200–300 mm Hg), moderate (PaO_2/FiO_2 = 100–200 mm Hg), and severe (PaO_2/FiO_2 ≤100 mm Hg). This framework redefined the former clinical entity of ALI as mild ARDS, restricting the term ALI to generalized pathophysiological descriptions or animal models. Crucially, despite advanced supportive strategies including lung-protective ventilation, neuromuscular blockers, and prone positioning, ARDS mortality has persisted at approximately 40% over the past two decades, underscoring the urgent need for improved therapeutic interventions.

Apoptosis is a selective physiological process of cell death, with the inflammatory response being a critical triggering factor. TNF-α, one of the earliest expressed inflammatory mediators, plays a crucial role in initiating and amplifying inflammatory responses.[19] This cytokine can promote cell apoptosis or necrosis by regulating the activation of caspase-9 or PIPK3, and it can also induce cell apoptosis through the death receptor pathway.[20,21] Research has demonstrated that inhibiting TNF-α production significantly reduces lung cell apoptosis in ALI mice.[22] Excessive production of IL-1β attracts more inflammatory cells to the lesion site, leading to the release of a large amount of pro-inflammatory mediators and triggering an inflammatory cascade. Research has confirmed that elevated levels of IL-1β suppress the proliferation of normal lung epithelial cells and induce apoptosis.[23] Lung epithelial cells serve as the first line of defense against harmful external substances, forming an airway barrier that inhibits the entry of pathogens, allergens, carcinogens, and other harmful compounds into the lungs, while preventing interstitial and vascular fluid leakage, maintaining gas exchange, and normal lung function.[24] Various lung diseases, such as chronic obstructive pulmonary disease, allergic asthma, and acute respiratory distress syndrome, are associated with damage to the airway barrier. Research has found that LPS can induce the aggregation and activation of neutrophils in the lungs, release reactive oxygen species and elastase, activate immune cells to secrete inflammatory mediators such as TNF-α, IL-1β, and IL-6, trigger an inflammatory cascade reaction, enhance caspase-3/9 activity, accelerate apoptosis of lung epithelial cells, and impair lung function.[25] Currently, the pathways of epithelial cell apoptosis include the PI3K/Akt pathway,[26] Fas/FasL,[27] and RIG-I-dependent signaling.[28] Intracellular apoptotic signaling pathways can be regulated through mitochondrial activation mediated by cytochrome C, apoptosis-inducing factors, and caspases, which are further modulated by members of the Bcl-2 protein family.[29] Previous studies have demonstrated that safflower yellow A treats ALI by inhibiting LPS-induced apoptosis in lung epithelial cells (Beas-2B).[30] Genipin pretreatment significantly activates the PI3K/AKT signaling pathway, reduces LPS-mediated mitochondrial apoptosis by down-regulating BAX and upregulating Bcl-2, improves mitochondrial dysfunction, inhibits caspase-3 activation, and prevents apoptosis.[31] During the progression of ALI, apoptosis of lung epithelial cells disrupts the integrity of the lung epithelial barrier, increases epithelial permeability, and results in fluid accumulation in the bronchi, ultimately leading to pulmonary edema.[32–34] Therefore, inhibiting

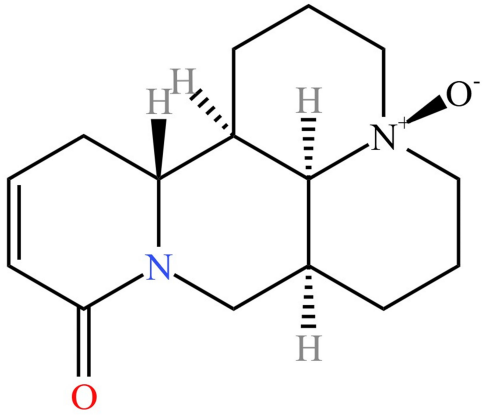

Figure 1 The structure of OSC.

neutrophil activation, reducing the secretion of pro-inflammatory cytokines, and alleviating lung epithelial cell apoptosis could be potential therapeutic strategies for treating ALI.

Oxysophocarpine (OSC, chemical structure shown in Figure 1) is a quinoline alkaloid primarily extracted from the leguminosae plants *Sophora flavescens* and *Sophora davidii*. It exhibits diverse pharmacological activities, including anti-inflammatory, anti-apoptotic, anticancer, antiarrhythmic, antiviral, and antibacterial effects.[35–42] Modern studies confirm that OSC, as a hydrophilic weak base drug, exhibits high solubility and permeability. It is absorbed primarily via passive diffusion through the gastrointestinal tract, demonstrating high oral bioavailability, thereby rendering it suitable for development as an oral dosage form. In traditional Chinese medicine (TCM), *Sophora flavescens* and *Sophora davidii* has been used for centuries for treating ulcers, skin burns, fevers, and inflammatory disorders. Previous study has demonstrated that OSC can effectively inhibit the proliferation and migration of oral squamous cell carcinoma cells by targeting the Nrf2/HO-1 axis.[43] Furthermore, OSC has shown significant antiviral activity by interfering with the NF-κB signaling pathway in human alveolar type II epithelial cells (A549) infected with respiratory syncytial virus, thereby reducing the production of pro-inflammatory cytokines and chemokines.[44] However, to date, there have been no comprehensive research reports specifically addressing the effects of OSC on ALI. The central objective of this research project is to explore the protective efficacy of OSC against ALI and to thoroughly elucidate its underlying mechanisms.

Materials and Methods

Mouse Modeling and Treatment

This experiment utilized female C57 mice, aged between 6–8 weeks, weighing (20±2) g. These mice were obtained from the Experimental Animal Center of Xi'an Jiaotong University School of Medicine. LPS (purity≥98%, 34231030001, Solarbio, Beijing, China) was employed to induce ALI in the mice. A total of 40 mice involved in the experiment and were randomly divided into four groups: normal control group, model group, low-dose OSC group (purity≥99.97%, 1104086, TargetMol, Shanghai, China) (20 mg/kg), and high-dose OSC group (40 mg/kg). Throughout the experiment, mice in the OSC groups received oral administration for 7 consecutive days. 1 hour after the last administration, LPS (30 mg/kg) was administered intranasally. 6 hours post LPS administration, the mice were anesthetized via intraperitoneal injection of pentobarbital sodium, followed by blood collection. The specific procedure was as follows: initially, eye blood was extracted through dissection, then centrifuged at 3000rpm for 10 minutes to collect serum. Subsequently, the bronchi and lungs of the mice were separated, with the left lung and upper respiratory tract ligated. A portion of the right lungs were thoroughly washed with physiological saline, and the lavage fluid was collected. The supernatant was obtained by centrifugation at 1000rpm for 10 minutes, aliquoted, and stored at −80°C. The left lung was divided into two parts; one was fixed with 4% paraformaldehyde (PFA), and the other was stored at −80°C. The entire experiment was conducted in strict accordance with the operating standards of the Shaanxi Provincial Institute of Traditional Chinese

Medicine and has been approved by the Animal Ethics Committee of the Shaanxi Provincial Institute of Traditional Chinese Medicine (SYDWLL-SQ-01).

Pathological Examination

The fixed lung tissues from each group were subsequently dehydrated using ethanol, made transparent with xylene, embedded in paraffin, and sectioned. Paraffin sections from each group were then stained using hematoxylin-eosin (HE, 20230427, Solarbio, Beijing, China). These stained sections were examined and photographed under an inverted microscope (Olympus, Japan) to evaluate the pathological changes in the lung tissues.

Lung wet-to-dry Weight Ratio

The severity of lung edema was evaluated by calculating the wet-to-dry weight ratio (W/D ratio) of lung tissue. The wet weight (W) of the lung tissue was immediately measured. Subsequently, the lung tissue was placed in a 60°C oven for 48 hours of drying treatment, and then reweighed to obtain the dry weight (D). The W/D ratio of the lung was determined by the ratio of the wet weight to the dry weight.

ELISA Assays

Following the guidelines provided by the ELISA kit (Fine Biotech, Wuhan, Hubei, China), the levels of cytokines TNF-α (EMC102a.96), IL-1β (EMC001b.96), and IL-6 (EMC004.96) in BALF were determined using sandwich ELISA. Briefly, 100 μL of standards or pre-diluted samples were added to antibody precoated 96-well plates, with blank control wells containing sample dilution buffer. After 90 min incubation at 37°C and two washes, 100 μL biotin conjugated detection antibody was added and incubated for 60 min at 37°C. Plates were washed three times (1 min soak per wash), followed by addition of 100 μL horseradish peroxidase (HRP)-streptavidin conjugate and 30-min incubation at 37°C. After five washes, 90 μL TMB substrate was added for 15 min of protected chromogenic reaction at 37°C. The reaction was terminated with 50 μL stop solution, and absorbance was measured at 450 nm within 15 min using a microplate reader. All incubations were strictly maintained at 37°C (non-CO_2 environment) with inter-step washes performed using prepared wash buffer.

Lung Tissue Apoptosis Staining

According to the instructions provided in the TUNEL cell apoptosis assay kit (SF594, 20231008, Solarbio, Beijing, China), the paraffin sections were deparaffinized twice in xylene and then subjected to a gradient treatment with ethanol-water solutions. Subsequently, the slices were incubated with proteinase K working solution for 20 minutes, followed by the addition of 50 μL of TUNEL reaction solution, which was incubated in the dark for 2 hours. Afterward, DAPI was used for counterstaining, with a staining time of 8 minutes. Finally, the sections were observed and photographed under an inverted fluorescence microscope (Olympus, Japan).

Cell Culture and Cell Viability Assay

The human lung epithelial cell line BEAS-2B was obtained from the ATCC China Cell Resource Center and cultured in a 37 °C, 5% CO2 incubator using DMEM medium supplemented with 10% fetal bovine serum, penicillin (100 IU/mL), and streptomycin (100 IU/mL).

For the experiment, cells were seeded in a 96-well plate at a density of 1×10^5 cells/well. After the cells adhered to the wall, the supernatant was discarded and replaced with 100 μL of DMEM medium containing varying concentrations (2.5–320 μg/mL) of OSC, with serum-free DMEM medium serving as the normal control group. Each concentration was set with 5 replicate wells. After 24 hours of incubation, an MTT solution (5 mg/mL) was added and the incubation continued for 4 hours. Subsequently, DMSO was added to dissolve the formazan crystals in the cells, and the absorbance was measured at 490 nm using an enzyme marker (Thermo Scientific, Singapore).

Cells were seeded in a 96-well plate at a density of 1×10^5 cells/well. After cell adhesion, OSC at concentrations of 40 μmol/L and 80 μmol/L was added for 6 hours, followed by co-incubation with LPS (40 μg/mL). After 24 hours, an MTT solution (5 mg/mL) was added and the incubation continued for 4 hours. Then DMSO was added to dissolve the

formazan crystals in the cells, and the absorbance was measured at 490 nm using an enzyme marker (Thermo Scientific, Singapore) to determine the effect of OSC on the viability of BEAS-2B cells under LPS stimulation.

$$\text{Cell Viability (\%)} = \text{Abs (Sample)}/\text{Abs (Control)} \times 100\%$$

Flow Cytometry

Bronchoalveolar lavage fluid (BALF) was centrifuged at 1000rpm for 10 minutes at 4°C to remove red blood cells. Subsequently, neutrophils in the BALF were labeled with CD11b and Ly6G for 20 minutes, followed by washing with PBS and analysis using a detection machine.

BEAS-2B lung epithelial cells in the logarithmic growth phase were seeded at a density of 1×10^5 cells/well in a 6-well plate. After 24 hours of incubation, the medium was changed, and the corresponding drugs were added. The following experimental groups were established: normal control group, LPS group, low-dose OSC group (40 μmol/L), and high-dose OSC group (80 μmol/L). After 24 hours of incubation, the OSC groups underwent OSC pretreatment for 6 hours. Subsequently, all three groups, except for the normal control group, were stimulated with LPS (40 μg/mL) for 24 hours. The cell culture supernatant was then collected into a centrifuge tube. The adherent cells were digested, and a cell suspension was prepared. After centrifugation, the cell supernatant was collected, and the upper layer of liquid was discarded. According to the instructions of the apoptosis detection kit (AK20058, Elabscience, Wuhan, Hubei, China), FITC and PI dyes were added and mixed thoroughly. The mixture was incubated at room temperature in the dark for 20 minutes. Finally, flow cytometry (Beckman, USA) was used to detect cell apoptosis.

Network Pharmacology Analysis

The OSC-related targets were searched for in the BATMAN database (http://bionet.ncpsb.org.cn/batman-tcm/index.php) and the Swiss Target Prediction database (http://swisstargetprediction.ch/). All targets were collected from the OMIM database (https://www.omim.org/), Drugbank database (https://go.drugbank.com/), and GeneCards database (https://www.genecards.org/) using the keywords "acute lung injury" and "airway epithelial cell apoptosis" separately. The search results were merged, and unique values were retained. The bioinformatics platform (https://www.bioinformatics.com.cn/) was used to draw a Venn diagram to obtain the intersection targets of "acute lung injury" and "airway epithelial cell apoptosis". The species was set to "Homo sapiens". The David platform was then utilized to perform Kyoto Encyclopedia of Genes and Genomes (KEGG) signal pathway enrichment analysis on the intersection targets. The 10 strongest associated signal pathways were analyzed and selected, followed by visualization on the bioinformatics platform. In this visualization, the redder the node, the smaller the P-value, and the larger the pathway, the more targets it contained. The intersection targets in the KEGG-enriched PI3K-Akt signaling pathway and Apoptosis pathway were imported into the STRING 11.5 database, with the species limited to Homo sapiens, to conduct protein interaction analysis. The results of this analysis were subsequently imported into Cytoscape 3.9.1 software for topological analysis, where a protein-protein interaction (PPI) network was constructed. The top 3 targets with the highest degree of freedom were then selected as the core targets.

Molecular Docking

The 3D structure file of the core target protein in PDB format was downloaded from the PDB database (https://www.rcsb.org/). Discovery Studio 4.5 Client software was then used to remove ligands and water molecules from the original structure. Next, compound files in PDB format were obtained from the Swiss Target Prediction platform, and the processed protein and compound files were imported into Autodock Tools (version 1.5.6) software. Subsequently, hydrogenation was performed on the molecules, charges were calculated, and the atomic types for the small molecules were specified. The protein's original ligand was used as the center of the docking box, and the size of the box was set to 80×80×80. Molecular docking was performed, and the docking results were visualized using PyMOL.

Western Blotting

Cell culture and grouping was performed in the same manner as 2.1. BEAS-2B cells were lysed using a radioimmunoprecipitation assay buffer (RIPA, Boster, Wuhan, China, prepared with 0.1 M PMSF and phosphatase inhibitor). The protein concentration was assessed using a BCA kit (111622230418, Beyotime, Shanghai, China). Subsequently, equal amounts of lysate samples (50 μg/lane) were separated by 10% SDS-PAGE electrophoresis, and the separated proteins were transferred onto PVDF membranes. At room temperature, the membranes were sealed with 5% skim milk for 1 hour, and then incubated overnight with specific primary antibodies at 4°C. The primary antibodies included: anti-KIT antibody (1:1000, Abcam), anti-p-PI3K antibody (1:700, ZEN-Bioscience), anti-PI3K antibody (1:700, ZEN-Bioscience), anti-Bcl-2 antibody (1:1000, Boster), and anti-BAX antibody (1:1000, Boster). After washing the membranes four times with TBST, the membranes were incubated with HRP-conjugated goat anti-rabbit IgG secondary antibody (1:2000, SAB) at 37°C for 1 hour, and washed again four times with TBST. Then, using chemiluminescence (ECL, Bio-Rad ChemiDoc XRS^{+}, USA), and the obtained images were analyzed by ImageJ software.

Immunofluorescence

Cell culture and grouping was performed in the same manner as 2.1. BEAS-2B cells were fixed with 4% PFA at room temperature for 15 minutes, followed by membrane permeabilization with 0.5% Triton X-100 at room temperature for 15 minutes. Next, sealed the cells with 10% goat serum at room temperature to avoid non-specific binding. Afterwards, overnight incubation was performed at 4 °C with primary antibodies. On the second day, cells were incubated with AF-488 fluorescently labeled secondary antibody (1:200) at 37°C in the dark for 1 hour, followed by DAPI staining for 5 minutes to label the cell nucleus. Finally, the fluorescence intensity changes of different cell components were observed and recorded using an inverted fluorescence microscope.

Real-Time Quantitative PCR

Cell culture and grouping was performed in the same manner as 2.1. Total RNA was extracted from the cells using Trizol reagent (AN93014A, TaKaRa, Japan). Subsequently, the SureScript™ First Strand cDNA Synthesis Kit (AMF2205A, Takara, Japan) was used for reverse transcription to synthesize cDNA. RT-qPCR amplification was performed with the following parameter settings: pre-denaturation at 95°C for 30s, followed by 40 cycles, each including denaturation at 95°C for 5 s, annealing at 60°C for 30s, and extension for 30s. GAPDH was used as an internal reference, and the relative expression levels of specific genes between each treatment group were analyzed using the $2^{-\Delta\Delta Ct}$ method. The primer sequences for specific genes are listed in Table 1.

Immunohistochemistry

The expressions of KIT, p-PI3K, Bcl-2, and BAX were evaluated in mouse lung tissues using immunohistochemistry method. According to the instructions of the KeyGEN One-Step IHC Assay (20210831, KeyGEN BioTECH, Nanjing, Jiangsu, China), the tissue sections were deparaffinized twice in xylene, followed by gradual dehydration in an ethanol gradient. Next, the sections were incubated in a 3% H_2O_2 solution for 10 minutes. At room temperature, 10% goat serum was applied for blocking. Subsequently, the sections were incubated separately with primary antibodies overnight at 4°C. After washing with PBS, the tissue sections were co-incubated with HRP-linked goat anti-rabbit IgG at room temperature

Table 1 Gene Primer Sequences

Gene	Source	Forward (5'-3')	Reverse (5'-3')
GAPDH	Human	TGCACCACCAACTGCTTAGC	TCTTCTGGGTGGCAGTGATG
PI3K	Human	CAGAACAATGCCTCCACGA	CACGGAGGCATTCTAAAGTC
KIT	Human	GTAAGGCTTACAACGATGTGGGCA	TTGAGCATCTTTACAGCGACAGTCA
Bcl-2	Human	GACTTCGCCGAGATGTCCAG	GAACTCAAAGAAGGCCACAATC
BAX	Human	CGAACTGGACAGTAACATGGAG	CAGTTTGCTGGCAAAGTAGAAA

for 30 minutes. Then, DAB was used for color development and counterstaining with hematoxylin. Finally, after dehydration, the sections were mounted and observed under a microscope.

Statistical Analysis

Statistical analysis was performed using SPSS 22.0 and GraphPad Prism software. All data were presented as the mean ± standard deviation (SD). Group differences were analyzed using one-way analysis of variance (ANOVA), and comparisons between two groups were made using an independent two-sample *t*-test. Statistical significance was set at $P < 0.05$.

Results

OSC Improved Pathologic Changes in an ALI Mouse Model

The pathological status of mouse lung tissues was evaluated through HE staining. The lung tissue structure of the normal group mice was intact, with cells arranged neatly and no obvious exudation in the alveoli. However, in LPS-induced mice, significant collapse and diffuse inflammatory cell infiltration were observed in the alveoli. Compared to the LPS model group, OSC treatment significantly reduced the infiltration of inflammatory cells (Figure 2A). Additionally, the lung W/D ratio of the LPS model group was higher than that of the normal group, whereas OSC treatment significantly reduced the lung W/D ratio, indicating that OSC could alleviate LPS-induced lung edema (Figure 2B). In the BALF of LPS-treated mice, the total number of cells was significantly higher than that of the normal group, while the total number of cells in the OSC-treated group was significantly lower than that of the model group (Figure 2C), suggesting that OSC improved inflammatory cell infiltration in LPS-induced ALI mice. Neutrophil infiltration is the most critical pathological feature of ALI. In the BALF of normal group mice, the proportion of neutrophils was 0.13±0.03%. In the LPS model group, the proportion of neutrophils significantly increased. Compared with the LPS model group, the administration of OSC (20 mg/kg or 40 mg/kg) decreased the proportion of neutrophils in the mouse BALF (Figure 2D and E). These results suggested that OSC reduced the accumulation of neutrophils in the lung tissue of ALI mice. The release of inflammatory factors is a typical pathological feature of ALI. Compared with the normal group, the levels of inflammatory factors TNF-α, IL-1β, and IL-6 in the BALF of the model group mice were significantly elevated ($p<0.05$). The levels of these inflammatory factors in the BALF of the OSC-treated group mice were significantly reduced compared to the model group ($p<0.05$). These results indicated that OSC alleviated LPS-induced ALI in mice by inhibiting the secretion of inflammatory factors in the lungs (Figure 2F and H).

OSC Exhibited Inhibition of Apoptosis in an ALI Mouse Model

Excessive apoptosis of lung tissue cells can lead to damage to the integrity of the epithelial barrier, exacerbating the inflammatory response and forming a malignant cycle. Compared to the normal group, the number of apoptotic cells in the lung tissues of LPS model group mice significantly increased, whereas the number of apoptotic cells in the lung tissues of OSC-treated group mice decreased significantly compared to the model group. This suggested that OSC had a protective effect against LPS-induced apoptosis in lung tissues (Figure 3A and B).

OSC Reduced Apoptosis of Pulmonary Epithelial Cells

The MTT results indicated that after incubating cells with varying concentrations (5–320 μmol/L) of OSC for 24 hours, there was no significant difference in the cell survival rate compared to the normal group (Figure 4A). The CCK-8 assay results demonstrated a significant decrease in cell viability in the LPS model group, while the groups treated with 80 μmol/L and 40 μmol/L OSC exhibited a significant increase in cell viability (Figure 4B). The results of Annexin V-FITC/PI double staining revealed that the proportions of Annexin V-FITC positive cells and PI positive cells in the normal group, model group, low-dose OSC group (40 μmol/L), and high-dose OSC group (80 μmol/L) were 0.94% ±0.04%, 4.23%±0.05%, 1.15%±0.05%, and 1.96%±0.03%, respectively. These findings indicated that LPS induced apoptosis in BEAS-2B cells, whereas OSC significantly mitigated LPS-induced apoptosis (Figure 4C).

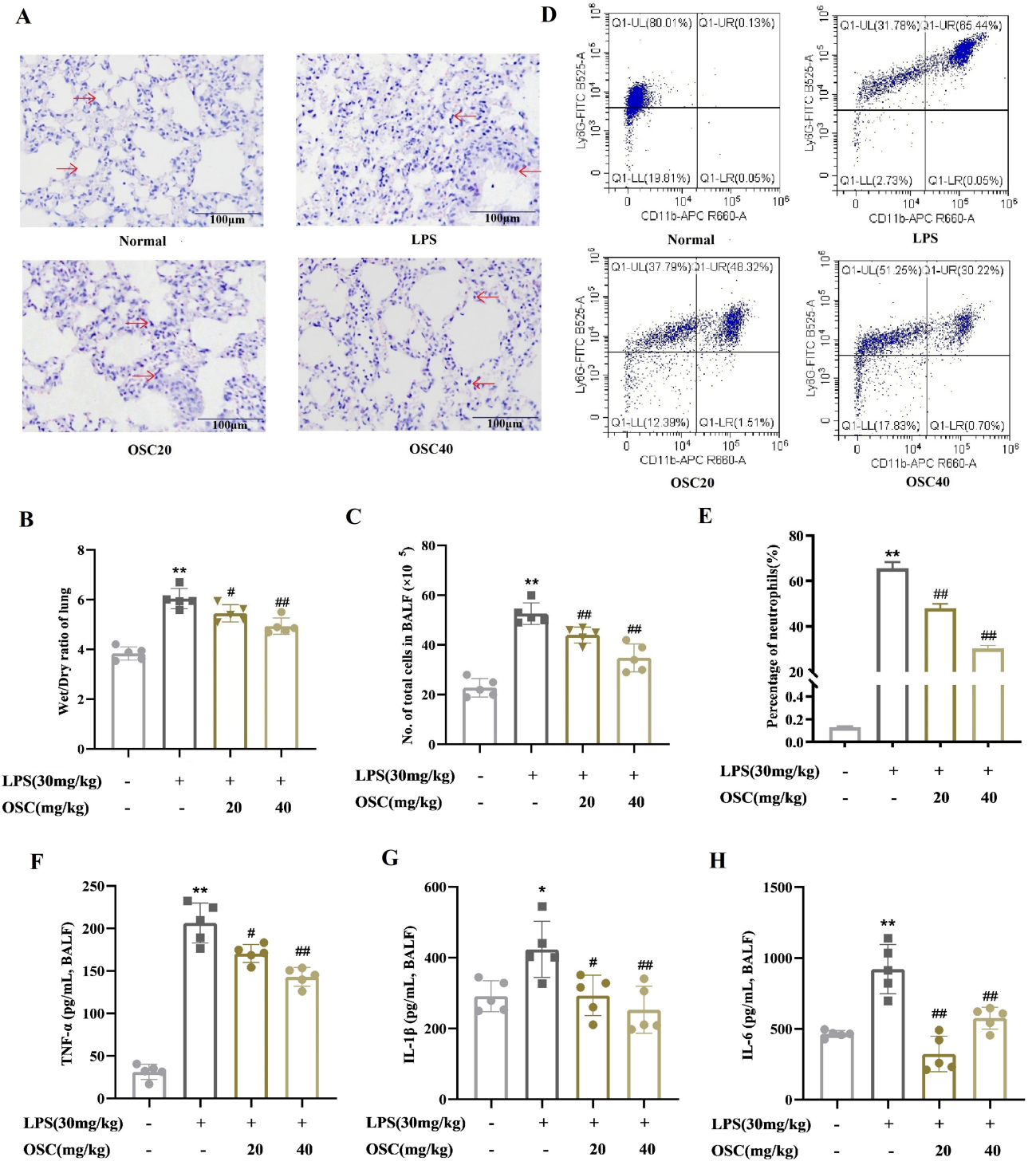

Figure 2 OSC attenuates histopathological changes in lungs of mice with acute lung injury. (**A**) HE staining detection of mouse air lung tissue sections. Magnification ×20. The red arrow indicates alveolar collapse and diffuse inflammatory cell infiltration. (**B**) Lung wet to dry weight ratio. (**C**) Total number of cells in BALF. (**D**) APC-FITC double staining to detect neutrophil accumulation in BALF. (**E**) Total number of neutrophil aggregates in BALF. (**F**) Levels of TNF-α in mouse BALF were determined by ELISA. (**G**) ELISA to determine the level of IL-1β in mouse BALF. (**H**) ELISA to determine the level of IL-6 in mouse BALF. Values are expressed as mean ± SD (n = 5). Compared with the Normal group, $^{*}p < 0.05$, $^{**}p < 0.01$; compared with the LPS model group, $^{\#}p < 0.05$, $^{\#\#}p < 0.01$. OSC exhibited inhibition of apoptosis in an ALI mouse model.

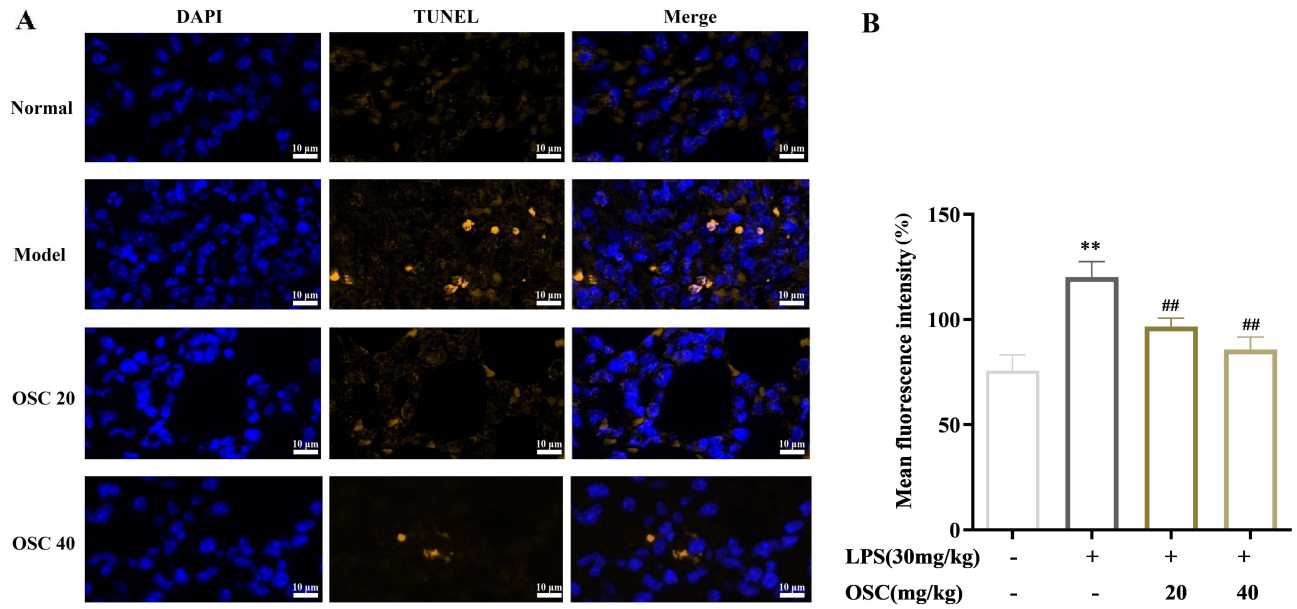

Figure 3 OSC exhibits inhibition of apoptosis in an ALI mouse model. (**A**) TUNEL staining to observe apoptosis of lung tissue cells. Magnification × 20. (**B**) Fluorescence intensity was analysed using Image J software. Values are expressed as mean ± SD (n = 5). $^{**}p < 0.01$ compared with Normal group; $^{\#\#}p < 0.01$ compared with LPS model group.

Network Pharmacology Prediction and Molecular Docking

Through the BATMAN and Swiss Target Prediction databases, a total of 263 targets related to OSC were identified. Meanwhile, 2289 targets related to ALI and 4614 targets related to airway epithelial cell apoptosis (AEC) were screened from the OMIM and Drugbank databases. Through Venn diagram analysis, it was found that there were 114 common targets between OSC and ALI, 160 common targets between OSC and AEC, and 1715 common targets between ALI and AEC. The intersection of the three revealed 106 common targets (Figure 5A). The KEGG pathway analysis results showed that 23 targets were enriched in the PI3K-Akt signaling pathway and apoptosis signaling pathway (Figure 5B). Through PPI analysis, KIT, PIK3CA, and Bcl-2 were identified as the core targets with the highest degrees of freedom (Figure 5C). These analyses revealed that OSC may activate the PI3K and Bcl-2 signaling pathways by binding to KIT on the cell surface, thereby regulating the process of cell apoptosis and providing protection for lung tissues (Figure 5D). The molecular docking experiment results further showed that the binding energies of OSC with KIT, PIK3CA, and Bcl-2 were −6.32, −7.84, and −7.92 kJ/mol, respectively (Figure 5E–G). These results indicated that OSC had strong binding effects with KIT, PIK3CA, and Bcl-2, suggesting that these targets were important in alleviating LPS-induced ALI by OSC.

OSC Upregulated the Expressions of KIT, p-PI3K, Bcl-2, and BAX

In the LPS-induced apoptosis model of BEAS-2B cells in vitro, compared with the normal group, LPS treatment significantly decreased the expressions of KIT, p-PI3K, and Bcl-2 proteins, while significantly increasing the expression of BAX protein. However, after OSC treatment, the expressions of KIT, p-PI3K, and Bcl-2 proteins significantly increased, while the expression of BAX protein significantly decreased (Figure 6A–L). At the mRNA level, compared with the normal group, the expressions of KIT, p-PI3K, and Bcl-2 mRNA in the model group significantly decreased, while the expression of BAX mRNA in the model group significantly elevated. Conversely, OSC treatment significantly increased the mRNA levels of p-PI3K, KIT, and Bcl-2 in BEAS-2B cells, while significantly reducing the mRNA level of BAX (Figure 6M–P).

KIT, PI3K, Bcl-2, and BAX proteins are key regulatory molecules in the KIT/PI3K signaling pathway. In the animal model of ALI, the number of yellow granules of p-PI3K, KIT, and Bcl-2 was lower in the lung tissue of mice, while the number of yellow granules of BAX was significantly elevated. In comparison, following high-dose and low-dose OSC treatments, there was a notable increase in the number of yellow granules corresponding to p-PI3K, KIT, and Bcl-2 in the lung tissue. Conversely, the number of yellow granules associated with BAX decreased (Figure 7). These findings

https://doi.org/10.2147/DDDT.S544479

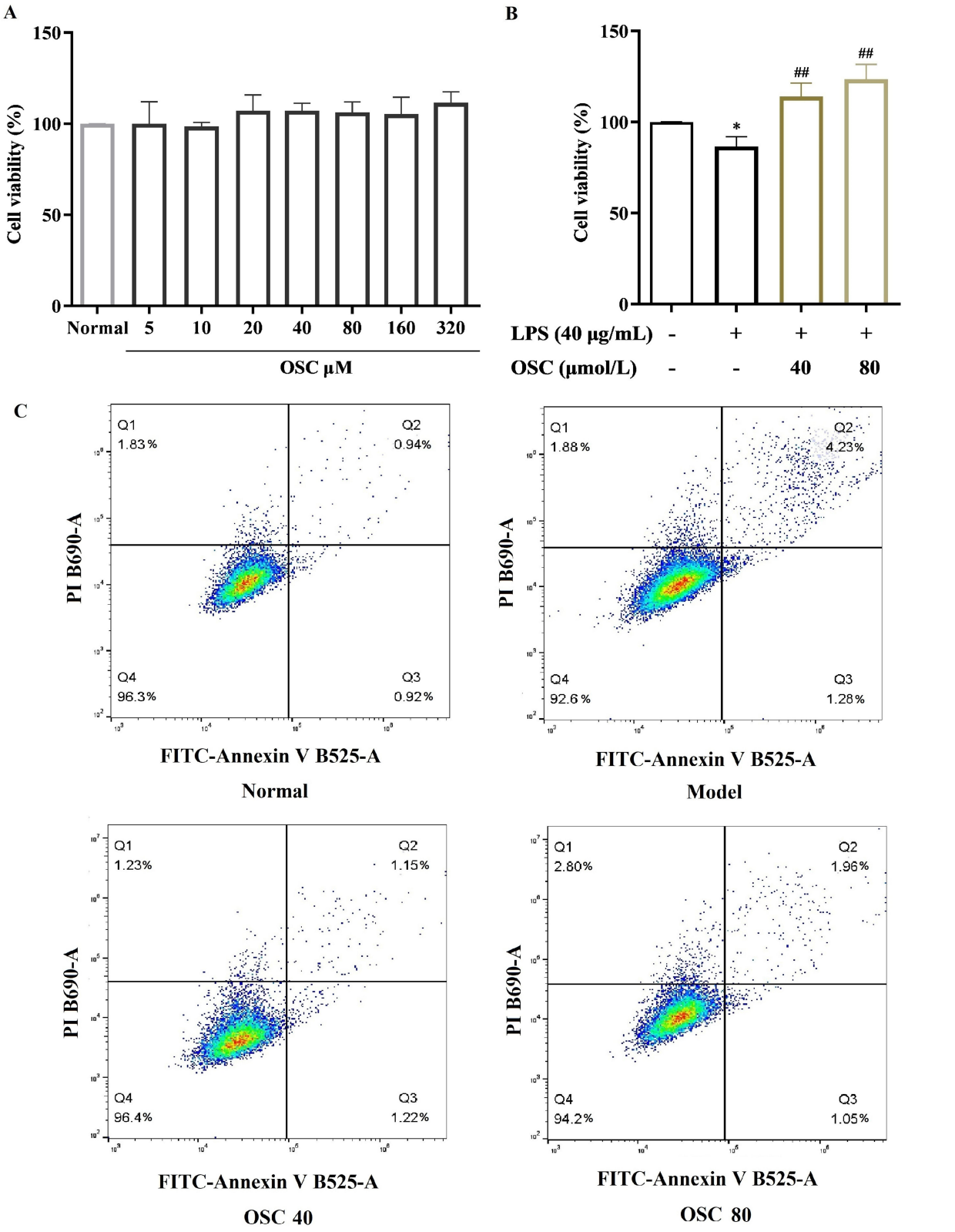

Figure 4 OSC Alleviates LPS-Induced Apoptosis of BEAS-2B Cells. (**A**) MTT assay to determine the effect of OSC on cell viability (n=5). (**B**) MTT assay to determine the effect of LPS on cell viability (n=5). (**C**) Annexin V/PI double staining to detect apoptosis of pulmonary epithelial cells. Values are expressed as mean±SD (n=3). *$p < 0.05$ compared with the Normal group; $^{\#\#}p < 0.01$ compared with the LPS model group.

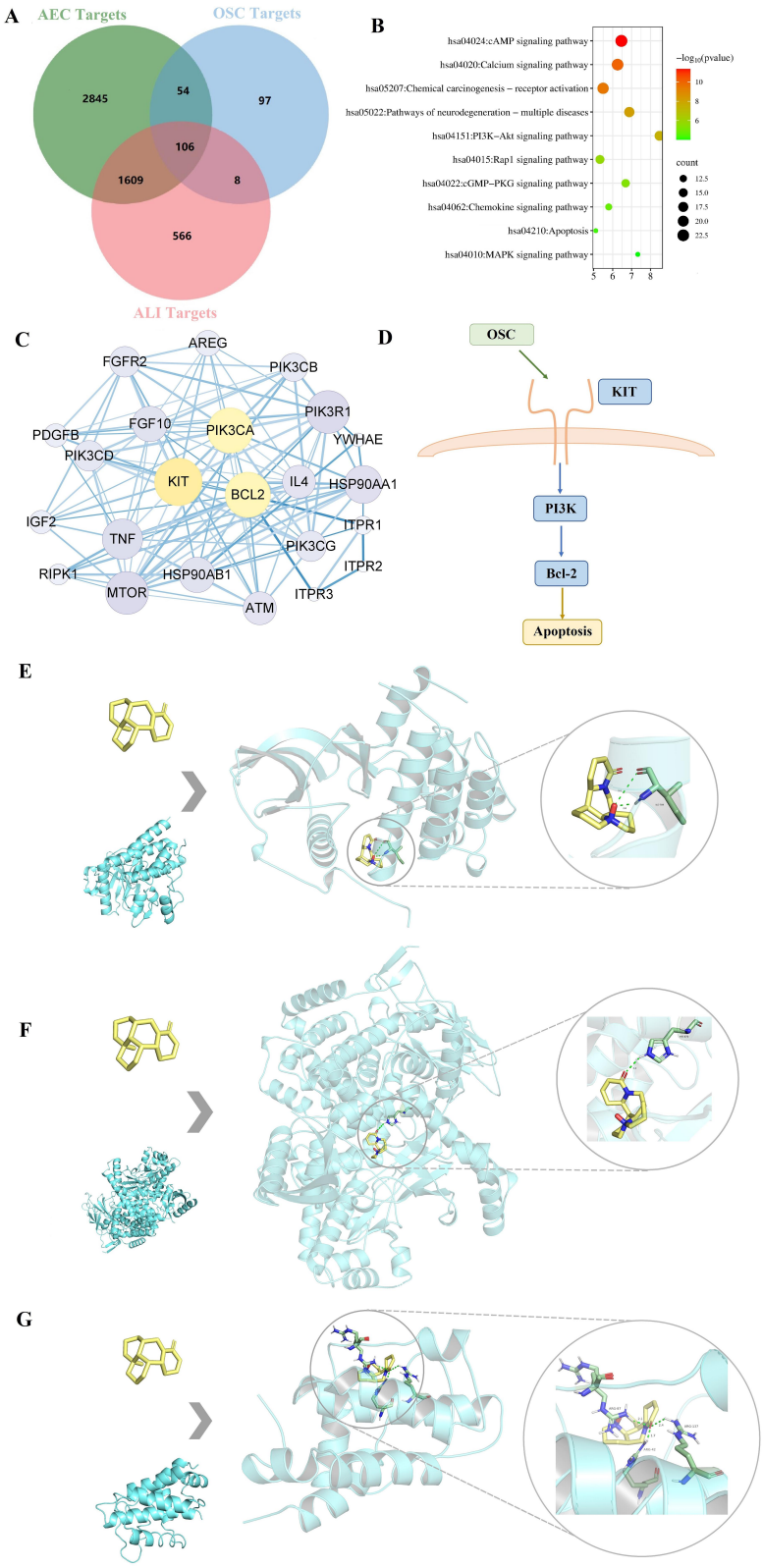

Figure 5 Network pharmacological analysis and molecular docking predicted the potential mechanism of OSC in alleviating epithelial cell apoptosis to treat acute lung injury. (**A**) Venn diagram of common targets between acute lung injury and pulmonary epithelial cell apoptosis. (**B**) KEGG pathway enrichment. (**C**) PPI protein interaction core target analysis. (**D**) Mechanism diagram of OSC alleviating epithelial cell apoptosis and reducing acute lung injury. (**E**) Molecular docking of OSC with KIT, binding energy of −6.32 kJ/mol. (**F**) Molecular docking of OSC with PIK3CA, binding energy of −7.84 kJ/mol. (**G**) Molecular docking of OSC with Bcl-2, binding energy of −7.92 kJ/mol.

https://doi.org/10.2147/DDDT.S544479

https://doi.org/10.2147/DDDT.S544479

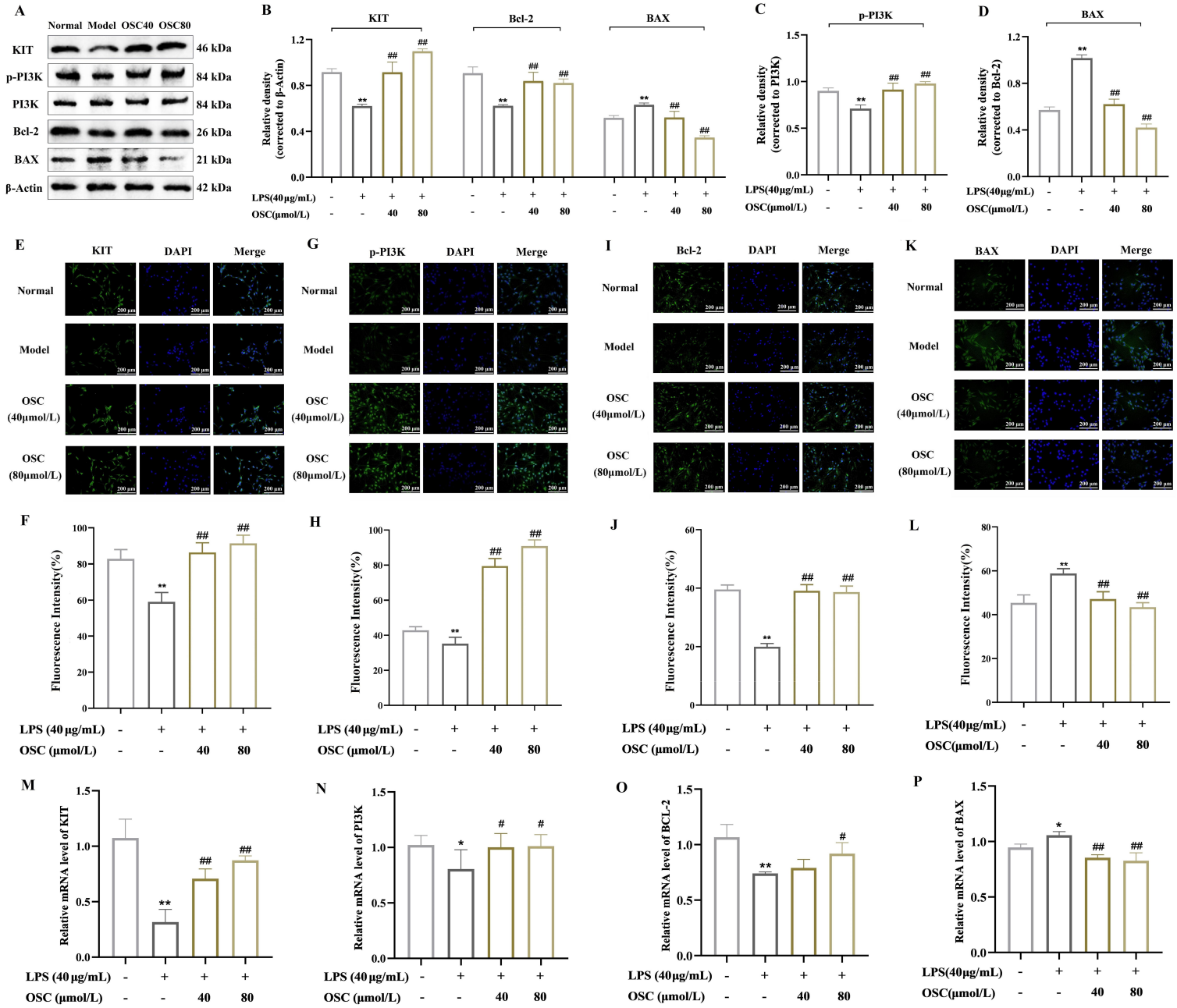

Figure 6 OSC regulates protein and mRNA expression of KIT, p-PI3K, Bcl-2 and BAX in LPS-induced BEAS-2B cells. (**A**) Western blotting for KIT, p-PI3K, PI3K, Bcl-2 and BAX protein expression in lungs. (**B**) Normalised quantitative data of KIT, Bcl-2 and BAX expression. β-Actin was used for normalisation. (**C**) Normalised quantitative data of p-PI3K expression. (**D**) Comparison of BAX/Bcl-2 ratio. (**E**) Immunofluorescence assay for KIT expression in BEAS-2B cells. (**F**) KIT fluorescence intensity was analysed using Image J software. (**G**) Detection of p-PI3K expression in BEAS-2B cells by immunofluorescence. (**H**) p-PI3K fluorescence intensity was analysed using Image J software. (**I**) Expression of Bcl-2 in BEAS-2B cells was detected by immunofluorescence. (**J**) Bcl-2 fluorescence intensity was analysed using Image J software. (**K**) Expression of BAX in BEAS-2B cells was detected by immunofluorescence. (**L**) BAX fluorescence intensity was analysed using Image J software. The figure shows blue fluorescence using DAPI as a nuclear dye, KIT protein shows blue fluorescence by AF488-labelled secondary antibody, and the merged image (Merge) demonstrates the effect of superimposition of two single-channel images. (**M**) Quantitative polymerase chain reaction results of KIT. (**N**) Quantitative polymerase chain reaction results of PI3K. (**O**) Quantitative polymerase chain reaction results of Bcl-2. (**P**) Quantitative polymerase chain reaction results for BAX. GAPDH was used for normalisation. Values are expressed as mean ± SD (n = 5). $^{*}p < 0.05$, $^{**}p < 0.01$ compared with the Normal group; $^{\#}p < 0.01$, $^{\#\#}p < 0.01$ compared with the LPS model group.

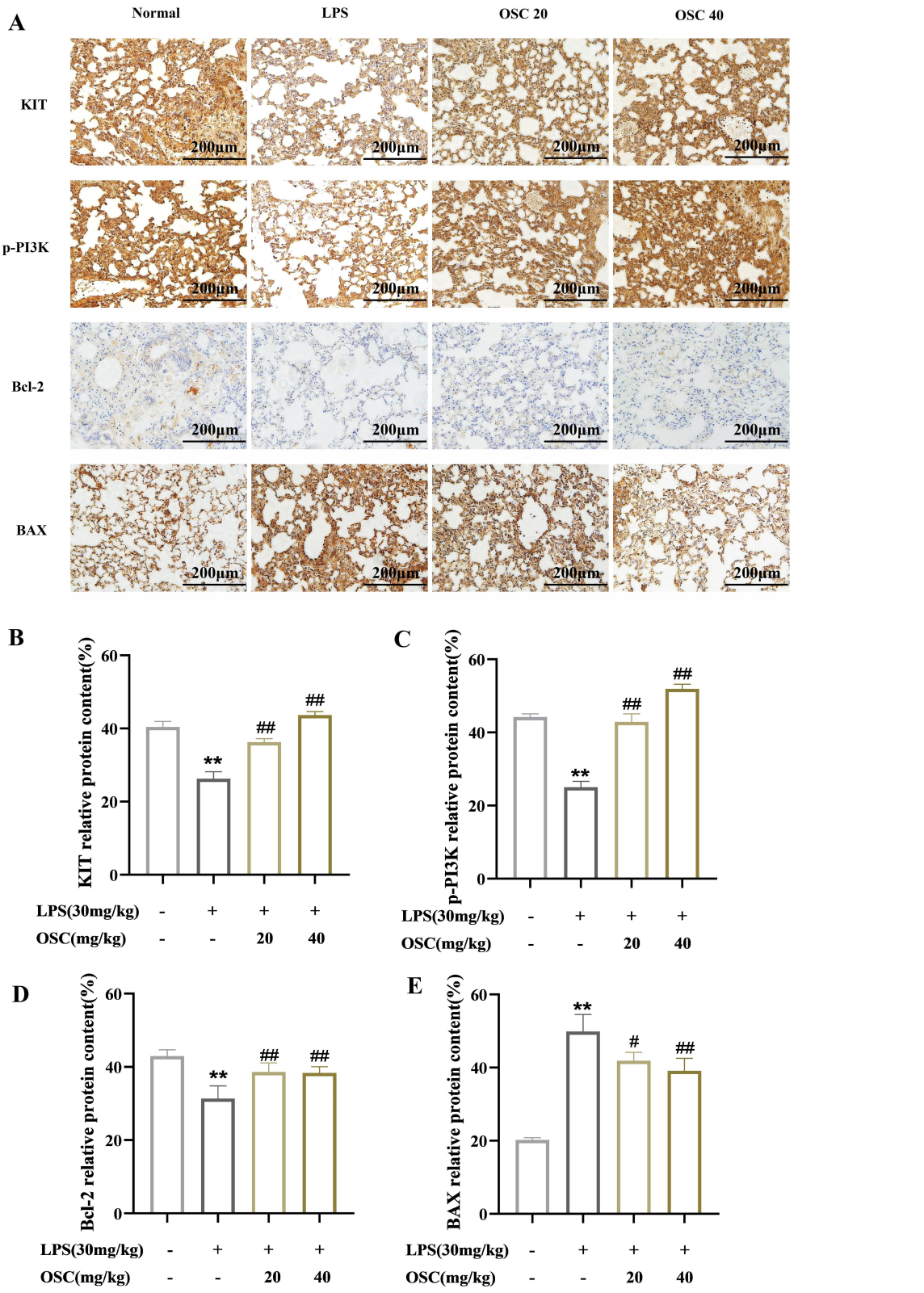

Figure 7 OSC regulates LPS-induced protein expression of KIT, p-PI3K, Bcl-2 and BAX in mouse lung tissues. (**A**) Representative images of immunohistochemical staining of KIT, p-PI3K, Bcl-2 and BAX in mouse lung tissue sections. Magnification ×20. (**B**) IHC method to determine the expression of KIT in lung tissues. (**C**) Expression of p-PI3K in lung tissues by ICH method. (**D**) ICH method to detect the expression of Bcl-2 in lung tissues. (**E**) Expression of BAX in lung tissues by ICH method. Values are expressed as mean ± SD (n = 5). $^{**}p < 0.01$ compared with the Normal group; $^{\#}p < 0.05$, $^{\#\#}p < 0.01$ compared with the LPS model group.

https://doi.org/10.2147/DDDT.S544479

suggested that OSC can effectively alleviate LPS-induced ALI by regulating the expression levels of p-PI3K and KIT proteins.

Discussion

ALI is a pathological condition caused by diverse diseases, including severe infection, trauma, shock, and burns. Its pathogenesis is intricate, and at present, there is no specific treatment available. In this study, we established LPS-induced ALI models and BEAS-2B cell apoptosis models in mice, revealing that OSC might alleviate ALI by regulating the KIT/PI3K signaling pathway.

ALI can be induced by multiple factors, such as infection and trauma, and is marked by the infiltration and activation of inflammatory cells, along with the overproduction of inflammatory factors.[45] TNF-α, as a potent pro-inflammatory cytokine, activates downstream transcription factors AP-1 and NF-κB via binding to TNFR1 or TNFR2, thereby mediating inflammatory responses.[46] Petrache et al[47] found that TNF-α promoted the apoptosis of rat lung epithelial cells by activating myosin light-chain kinase and Rho-associated kinase, increasing myosin light chain phosphorylation, and regulating the caspase-8 substrate.[48] In our study, we found OSC inhibited the TNF-α secretion, which contribute to anti-inflammation. Research also showed that the combined action of TNF-α and IFN-β activated caspase-8 and caspase-3, leading to the apoptosis of BEAS-2B cells.[49] IL-1β can be secreted by activated epithelial cells, and the secretion process is regulated by the Toll-like receptor, Nod-like receptor pathways, and the caspase-1 pathway.[50] Pyrrole DTA0118 can alleviate ALI by reducing the expression of TLR4 receptors and down-regulating the secretion of IL-1β in LPS-induced human lung epithelial BEAS-2B cells.[51] Additionally, significantly alleviated the severity of LPS-induced ALI in mice by inhibiting the production of IL-1β in BALF.[52] Eldredge et al[49] found that IL-6 levels were significantly elevated in patients with lung injury. In this study, we observed a significant increase in IL-1β, and IL-6 levels in the BALF of LPS-induced ALI mice, while OSC treatment significantly reduced the levels of these inflammatory factors, indicating that OSC can effectively alleviate the inflammatory response in ALI.

Interstitial edema and neutrophil aggregation caused by inflammatory outbreaks are typical features of ALI.[53] Various inflammatory factors lead to diffuse alveolar damage, disrupt the epithelial-endothelial barrier, and cause excessive leakage of protein-rich fluids and blood cells into the interstitium and alveoli, resulting in interstitial edema.[54] Our study found that OSC significantly reduced the lung W/D ratio induced by LPS by inhibiting diffuse alveolar damage in ALI mice, thereby effectively alleviating lung edema. Under normal physiological conditions, neutrophils adhere to the endothelium of alveolar capillaries. When inflammation occurs, they become activated, cross the alveolar capillary endothelium, and accumulate at the site of the inflammatory response. Activated neutrophils secrete various inflammatory factors and reactive oxygen species, which further exacerbate ALI.[55] Flavonoid esculin reduces the total number of cells and neutrophils in BALF, alleviating LPS-induced lung pathological damage.[56] Our study also found that OSC treatment significantly reduced the proportion and aggregation of neutrophils in the BALF of LPS-induced ALI mice. Thus, OSC may have a protective effect on lung tissue by modulating neutrophil aggregation and reducing lung edema.

Lung epithelial cells play a crucial role in maintaining the functional integrity of the lung epithelial barrier.[57,58] Research has found that LPS significantly reduces the viability of lung epithelial cells and induces excessive cell apoptosis.[59] Uncontrolled cell apoptosis can trigger inflammatory responses, causing lung tissue damage. Irisin has been shown to alleviate LPS-induced apoptosis in rat lung tissue cells and improve LPS-induced dysfunction of the alveolar epithelial barrier.[60] Additionally, hexokinase 2 reduces LPS-induced apoptosis in human lung epithelial BEAS-2B cells by inhibiting the mitochondrial apoptosis pathway. In this study, we found that OSC pretreatment significantly improved the viability and reduced LPS-induced apoptosis in BEAS-2B cells. In summary, previous studies and our experimental results suggested that the alleviating effect of OSC on ALI might be related to its ability to reduce lung epithelial cell apoptosis.

Combining network pharmacology with in vitro and in vivo experiments is an important method for studying disease mechanisms and drug effects.[61,62] Li N et al predicted through network pharmacology that kaempferol (KA) and ginsenoside Rg1 (GRg1) may treat ALI by targeting AKT1, PIK3R1, PTK2, and STAT3 in the PI3K-AKT signaling pathway. This prediction was validated through rat experiments, which showed that treatment with KA and GRg1 significantly inhibited the activity of PI3K and AKT1.[63] In this study, we identified 106 common targets using "lung

epithelial cell apoptosis" and "acute lung injury" as keywords. Through KEGG enrichment analysis and PPI analysis, we predicted KIT, PIK3CA, and Bcl-2 as core targets. The molecular docking results further indicated that OSC had a strong binding affinity with KIT, PIK3CA, and Bcl-2, suggesting that these proteins may have been key molecules through which OSC alleviated ALI by regulating the KIT/PI3K signaling pathway. PI3K is a crucial component of the PI3K-Akt pathway, influencing cell proliferation, differentiation, and migration, and the activation of downstream transcription factors that stimulate the release of pro-inflammatory cytokines.[64] C-kit, a receptor for stem cell factor (SCF), regulates cell proliferation, differentiation, and apoptosis through specific binding with SCF. As an upstream molecule of the PI3K/Akt pathway, C-kit can activate the PI3K/Akt pathway through homodimerization upon binding to its ligand, SCF.[65] Liensinine inhibits LPS-induced apoptosis in BEAS-2B cells by down-regulating proteinase-3 and Bcl-2-associated X proteins, while menthol inhibits LPS-induced apoptosis of alveolar epithelial cells by regulating the PI3K/Akt pathway.[30] Our study found that in the LPS-induced BEAS-2B cell model, the expression levels of PI3K, c-KIT, and Bcl-2 were significantly reduced, while OSC pretreatment increased their expressions. Similarly, in mouse lung tissues, the expressions of PI3K, c-KIT, and Bcl-2 diminished under LPS induction, but OSC treatment elevated their expression levels. These findings indicate that OSC mitigate ALI and has potential value for the development of clinical therapeutic drugs. However, the protective effects of OSC only were demonstrated in animal models. There are still many problems and limitations in its development into clinical drugs. For example, oxysophocarpine is currently mainly extracted from traditional Chinese medicinal materials, and this method of acquisition is inefficient and costly. This study mainly focuses on research based on inflammation reduction. However, the pathogenesis of acute lung injury is complex, and enhanced oxidative stress is another key pathogenic mechanism. Future research should prioritize addressing these limitations to advance this discovery toward clinical translation.

Conclusion

This study indicated that OSC administration reduced LPS-induced neutrophil infiltration in ALI mice, inhibited the secretion of pro-inflammatory cytokines (TNF-α, IL-1β, and IL-6), lowered the W/D ratio of the lungs, alleviated lung tissue cell apoptosis, and improved lung function. Through network pharmacology and molecular docking analysis, we predicted that the KIT/PI3K pathway played a key role in OSC's inhibition of cell apoptosis and alleviation of ALI. Further mechanistic studies showed that OSC reduced LPS-induced apoptosis in BEAS-2B lung epithelial cells and increased PI3K, c-KIT, and Bcl-2 expressions. In summary, we have preliminarily revealed the molecular mechanism of OSC in preventing and treating ALI, which may be related to its regulation of the KIT/PI3K signaling pathway, reduction of the inflammatory response, and modulation of lung epithelial cell apoptosis. At present, the clinical treatment of ARDS is still based on mechanical ventilation and other supportive treatment. Glucocorticoids, neuromuscular blockers and β2 receptor agonists have been used in drug treatment, but they have not been proved to continuously improve the clinical prognosis. Traditional Chinese medicine provides a new treatment idea for ARDS with its multi-component, multi-link and multi-target therapeutic advantages. This study offers valuable insights supporting the clinical application of OSC, highlighting its potential significance in exploring the use of traditional Chinese medicine for treating ALI/ARDS.

Abbreviations

ALI, Acute lung injury; LPS, Lipopolysaccharide; ARDS, Acute respiratory distress syndrome; OSC, Oxysophocarpine; TNF-α, Tumor necrosis factor; IL-1β, Interleukin 1 Beta; IL-6, Interleukin 6; Bcl-2, B-cell lymphoma-2; BAX, Bcl-2 Associated X Protein; PI3K, Phosphatidylinositol 3-kinase; BALF, Bronchoalveolar lavage fluid; KEGG, Kyoto Encyclopedia of Genes and Genomes; PPI, protein-protein interaction.

Data Sharing Statement

The data used to support the findings of this study are all provided. The data is provided on request from corresponding author.

Ethics Approval and Consent to Participate

There are no Ethical issues/concerns relating to this work.

Consent for Publication

All authors concur with the submission and publication of this paper.

Acknowledgments

Ziyao Qiao and Kaihua Long are co-first authors for this study. All opinions expressed in this article are those of the authors and do not necessarily represent the views of their affiliates or of the publisher, editors and reviewers. Any products that may be evaluated herein, or any claims that may be made by their manufacturers, are not warranted or endorsed by the publisher.

Author Contributions

All authors made a significant contribution to the work reported, whether that is in the conception, study design, execution, acquisition of data, analysis and interpretation, or in all these areas; took part in drafting, revising or critically reviewing the article; gave final approval of the version to be published; have agreed on the journal to which the article has been submitted; and agree to be accountable for all aspects of the work.

Funding

This research was funded by study of Key Research and Development Program of Shaanxi (Program No. 2021ZDLSF04-06 and No. 2022ZDXM-SF-06), Shaanxi Provincial Administration of Traditional Chinese Medicine Project (Program No. 2021-QYZL-01, SZY-KJCYC-2025-ZY-005, TZKZ-CXRC-05, 2025-CXTD-11), Natural Science Foundation of Shaanxi Province (Program no. 2023-JC-QN-0820), Science and Technology Planning Project of Xi'an (no. 23YXYJ0165).

Disclosure

The authors declare that they have no conflicts of interest in this work.

References

1. Gouda MM, Bhandary YP. Acute lung injury: IL-17A-mediated inflammatory pathway and its regulation by curcumin. *Inflammation*. 2019;42(4):1160–1169. doi:10.1007/s10753-019-01010-4
2. Long ME, Mallampalli RK, Horowitz J. Pathogenesis of pneumonia and acute lung injury. *Clin Sci*. 2022;136(10):747–769. doi:10.1042/cs20210879
3. Huang XT, Liu W, Zhou Y, et al. Galectin-1 ameliorates lipopolysaccharide-induced acute lung injury via AMPK-Nrf2 pathway in mice. *Free Radic Biol Med*. 2020;146:222–233. doi:10.1016/j.freeradbiomed.2019.11.011
4. Seth Kligerman M. Pathogenesis, imaging, and evolution of acute lung injury. *Radiol Clin North Am*. 2022;60(6):925–939. doi:10.1016/j.rcl.2022.06.005
5. Gordon D, Rubenfeld MD, Caldwell MSE, et al. Incidence and outcomes of acute lung injury. *N Engl J Med*. 2005;353(16):1685–1693. doi:10.1056/NEJMoa050333
6. Komiya K, Akaba T, Kozaki Y, et al. A systematic review of diagnostic methods to differentiate acute lung injury/acute respiratory distress syndrome from cardiogenic pulmonary edema. *Crit Care*. 2017;21(1):228. doi:10.1186/s13054-017-1809-8
7. Mokra D, Mikolka P, Kosutova P, et al. Corticosteroids in acute lung injury: the dilemma continues. *Int J Mol Sci*. 2019;20(19):4765. doi:10.3390/ijms20194765
8. Zeiher BG, Matsuoka S, Kawabata K, et al. Neutrophil elastase and acute lung injury: prospects for sivelestat and other neutrophil elastase inhibitors as therapeutics. *Crit Care Med*. 2002;30(Supplement):S281–S87. doi:10.1097/00003246-200205001-00018
9. Singla S, Jacobson JR. Statins as a novel therapeutic strategy in acute lung injury. *Pulm Circ*. 2012;2(4):397–406. doi:10.4103/2045-8932.105028
10. Slutsky AS. History of mechanical ventilation: from vesalius to ventilator-induced lung injury. *Am J Respir Crit Care Med*. 2015;191(10):1106–1115. doi:10.1164/rccm.201503-0421PP
11. Wang K, Wang MY, Liao XM, et al. Locally organised and activated Fth1hi neutrophils aggravate inflammation of acute lung injury in an IL-10-dependent manner. *Nat Commun*. 2022;13(1):7703. doi:10.1038/s41467-022-35492-y
12. D'Alessio FR. Mouse models of acute lung injury and ARDS. *Methods Mol Biol*. 2018;1809:341–350. doi:10.1007/978-1-4939-8570-8_22
13. Ciesielska A, Matyjek M, Kwiatkowska K. TLR4 and CD14 trafficking and its influence on LPS-induced pro-inflammatory signaling. *Cell Mol Life Sci*. 2020;78:1233–1261. doi:10.1007/s00018-020-03656-y

14. Li D, Guo YY, Cen XF, et al. Lupeol protects against cardiac hypertrophy via TLR4-PI3K-Akt-NF-κB pathways. *Acta Pharmacol Sin*. 2021;43(8):1989–2002. doi:10.1038/s41401-021-00820-3
15. Karunakaran D, Nguyen M-A, Geoffrion M. RIPK1 expression associates with inflammation in early atherosclerosis in humans and can be therapeutically silenced to reduce NF-κB activation and atherogenesis in mice. *Circulation*. 2021;143(2):163–177. doi:10.1161/CIRCULATIONAHA.118.038379
16. Kong D, Yamori T. Advances in development of phosphatidylinositol 3 kinase inhibitors. *Curr Med Chem*. 2009;16(22):2839–2854. doi:10.2174/092986709788803222
17. Inanir S, Copoglu US, Kokacya H, et al. Agomelatine protection in an LPS-induced psychosis-relevant behavior model. *Med Sci Monit*. 2015;21:3834–3839. doi:10.12659/msm.895505
18. Wang YY, Wang X, Li YX, et al. Xuanfei Baidu Decoction reduces acute lung injury by regulating infiltration of neutrophils and macrophages via PD-1/IL17A pathway. *Pharmacol Res*. 2022;176:106083. doi:10.1016/j.phrs.2022.106083
19. Raymondos K, Martin MU, Schmudlach T, et al. Early alveolar and systemic mediator release in patients at different risks for ARDS after multiple trauma. *Injury*. 2012;43(2):189–195. doi:10.1016/j.injury.2011.05.034
20. Cicha I, Urschel K. TNF-α in the cardiovascular system: from physiology to therapy. *Int J Interferon Cytokine Mediat Res*. 2015;7:9–25. doi:10.2147/ijicmr.s64894
21. Wajant H, Scheurich P. TNFR1-induced activation of the classical NF-κB pathway. *FEBS J*. 2011;278(6):862–876. doi:10.1111/j.1742-4658.2011.08015.x
22. Lau KS, Juchheim AM, Cavaliere KR, et al. In vivo systems analysis identifies spatial and temporal aspects of the modulation of TNF-{alpha}-induced apoptosis and proliferation by MAPKs. *Sci Signal*. 2011;4(165):ra16. doi:10.1126/scisignal.2001338]
23. Kühnapfel A, Horn K, Klotz U, et al. Genetic regulation of cytokine response in patients with acute community-acquired pneumonia. *Genes*. 2022;13(1):111. doi:10.3390/genes13010111
24. Shenoy AT, Lyon De Ana C, Arafa EI, et al. Antigen presentation by lung epithelial cells directs CD4+ TRM cell function and regulates barrier immunity. *Nat Commun*. 2021;12(1):5834. doi:10.1038/s41467-021-26045-w
25. Zhou HC, Wang XH, Zhang B. Depression of lncRNA NEAT1 antagonizes LPS-evoked acute injury and inflammatory response in alveolar epithelial cells via HMGB1-RAGE signaling. *Mediators Inflamm*. 2020;2020:1–11. doi:10.1155/2020/8019467
26. García-Cuellar CM, Chirino YI, Morales-Bárcenas R, et al. Airborne particulate matter (PM10) inhibits apoptosis through PI3K/AKT/FoxO3a pathway in lung epithelial cells: the role of a second oxidant stimulus. *Int J Mol Sci*. 2020;21(2):473. doi:10.3390/ijms21020473
27. Jiang HB, Wang SM, Hou LK, et al. Resveratrol inhibits cell apoptosis by suppressing long noncoding RNA (lncRNA) XLOC_014869 during lipopolysaccharide-induced acute lung injury in rats. *J Thorac Dis*. 2021;13:6409–6426. doi:10.21037/jtd-21-1113
28. Gracemary LRY, Sachaphibulkij K, Foo SL, et al. Annexin-A1 promotes RIG-I-dependent signaling and apoptosis via regulation of the IRF3–IFNAR–STAT1–IFIT1 pathway in A549 lung epithelial cells. *Cell Death Dis*. 2020;11(6):463. doi:10.1038/s41419-020-2625-7
29. Sun R, Jiang KM, Zeng CY, et al. Synergism of TNF-α and IFN-β triggers human airway epithelial cells death by apoptosis and pyroptosis. *Mol Immunol*. 2023;153:160–169. doi:10.1016/j.molimm.2022.12.002
30. Chen LS, Zheng D-S. Safflor yellow A protects beas-2B cells against LPS-induced injury via activating Nrf2. *Rev Bras Farmacogn*. 2023;33(4):802–811. doi:10.1007/s43450-023-00409-3
31. Luo X, Lin B, Gao YG, et al. Genipin attenuates mitochondrial-dependent apoptosis, endoplasmic reticulum stress, and inflammation via the PI3K/AKT pathway in acute lung injury. *Int Immunopharmacol*. 2019;76:105842. doi:10.1016/j.intimp.2019.105842
32. Si ZY, Zhang B. Amygdalin attenuates airway epithelium apoptosis, inflammation, and epithelial-mesenchymal transition through restraining the TLR4/NF-κB signaling pathway on LPS-treated BEAS-2B bronchial epithelial cells. *Int Arch Allergy Immunol*. 2021;182(10):997–1007. doi:10.1159/000514209
33. Liu CX, Wang JM, Tan YR, et al. CTNNAL1 promotes the structural integrity of bronchial epithelial cells through the RhoA/ROCK1 pathway. *Acta Biochim Biophys Sin*. 2024;56(5):753–762. doi:10.3724/abbs.2024026
34. Wang LN, Zhang YX, Song ZM, et al. Ginsenosides: a potential natural medicine to protect the lungs from lung cancer and inflammatory lung disease. *Food Funct*. 2023;14(20):9137–9166. doi:10.1039/d3fo02482b
35. Gough KC, Maddison BC, Shikotra A, et al. Evidence for a novel Kit adhesion domain mediating human mast cell adhesion to structural airway cells. *Respir Res*. 2015;16(1):86. doi:10.1186/s12931-015-0245-z
36. Suzuki T, Tada Y, Nishimura R, et al. Endothelial-to-mesenchymal transition in lipopolysaccharide-induced acute lung injury drives a progenitor cell-like phenotype. *Am J Physiol Lung Cell Mol Physiol*. 2016;310(11):L1185–L98. doi:10.1152/ajplung.00074.2016
37. Zhi WB, Jiang SN, Xu ZR, et al. Oxysophocarpine inhibits airway inflammation and mucus hypersecretion through JNK/AP-1 pathway in vivo and in vitro. *Fitoterapia*. 2022;162:105278. doi:10.1016/j.fitote.2022.105278
38. Li LF, Shi RB, Shi WM, et al. Oxysophocarpine protected airway epithelial cells against inflammation and apoptosis by inhibiting miR-155 expression. *Future Med Chem*. 2020;12:1475–1487. doi:10.4155/fmc-2020-0120
39. Zhao JY, Wang ZM, Yi H, et al. Discussion on rationality of Yinpian commodity grades--Sophora flavescentis as an example. *China J Chinese Materia Medica*. 2021;46(16):4040–4050. doi:10.19540/j.cnki.cjcmm.20210507.302
40. Roh SS, Kim CD, Lee MH, et al. The hair growth promoting effect of Sophora flavescens extract and its molecular regulation. *J Dermatol Sci*. 2002;30(1):43–49. doi:10.1016/s0923-1811(02)00060-9
41. Yang Y, Li YX, Wang HL, et al. Oxysophocarpine ameliorates carrageenan-induced inflammatory pain via inhibiting expressions of prostaglandin E2 and cytokines in mice. *Planta Med*. 2015;81(10):791–797. doi:10.1055/s-0035-1546153
42. Huang X, Lowrie DB, Fan X-Y, et al. Natural products in anti-tuberculosis host-directed therapy. *Biomed Pharmacother*. 2024;171:116087. doi:10.1016/j.biopha.2023.116087
43. Liu R, Peng J, Wang H, et al. Oxysophocarpine retards the growth and metastasis of oral squamous cell carcinoma by targeting the Nrf2/HO-1 axis. *Cell Physiol Biochem*. 2018;49(5):1717–1733. doi:10.1159/000493615
44. Shi X, Gao T, Yu C, et al. Oxysophocarpine attenuates inflammatory osteolysis by modulating the NF-κb pathway and the reactive oxygen species-related Nrf2 signaling pathway. *Inflammopharmacology*. 2024;32(5):3461–3474. doi:10.1007/s10787-024-01552-6
45. Li YR, Jiang YN, Zhang H, et al. Research on acute lung injury inflammatory network. *Int J Clin Pharmacol Ther*. 2023;61:394–403. doi:10.5414/cp204438

46. Baud V, Karin M. Signal transduction by tumor necrosis factor and its relatives. *Trends Cell Biol*. 2001;11(9):372–377. doi:10.1016/s0962-8924(01)02064-5
47. Petrache I, Verin AD, Crow MT, et al. Differential effect of MLC kinase in TNF-α-induced endothelial cell apoptosis and barrier dysfunction. *Am J Physiol Lung Cell Mol Physiol*. 2001;280(6):L1168–L78. doi:10.1152/ajplung.2001.280.6.L1168
48. An SC, Hishikawa Y, Liu J, et al. Lung injury after ischemia-reperfusion of small intestine in rats involves apoptosis of type II alveolar epithelial cells mediated by TNF-α and activation of Bid pathway. *Apoptosis*. 2007;12(11):1989–2001. doi:10.1007/s10495-007-0125-1
49. Eldredge LC, Creasy RS, Tanaka S, et al. Imbalance of Ly-6Chi and Ly-6Clo monocytes/macrophages worsens hyperoxia-induced lung injury and is rescued by IFN-γ. *J Immunol*. 2019;202(9):2772–2781. doi:10.4049/jimmunol.1801374
50. Kroemer G, Galluzzi L, Vandenabeele P, et al. Classification of cell death: recommendations of the nomenclature committee on cell death 2009. *Cell Death Differ*. 2008;16(1):3–11. doi:10.1038/cdd.2008.150
51. Cabrera-Benítez NE, Pérez-Roth E, Ramos-Nuez Á, et al. Inhibition of endotoxin-induced airway epithelial cell injury by a novel family of pyrrol derivates. *Lab Invest*. 2016;96(6):632–640. doi:10.1038/labinvest.2016.46
52. Mei SH, McCarter SD, Deng Y, Parker CH, Liles WC, Stewart DJ. Prevention of LPS-induced acute lung injury in mice by mesenchymal stem cells overexpressing angiopoietin 1. *PLoS Med*. 2007;4(9):e269. doi:10.1371/journal.pmed.0040269
53. Hughes KT, Beasley MB. Pulmonary manifestations of acute lung injury: more than just diffuse alveolar damage. *Arch Pathol Lab Med*. 2017;141(7):916–922. doi:10.5858/arpa.2016-0342-RA
54. Cong Z, Yang C, Zeng Z, et al. α1-adrenoceptor stimulation ameliorates lipopolysaccharide-induced lung injury by inhibiting alveolar macrophage inflammatory responses through NF-κB and ERK1/2 pathway in ARDS. *Front Immunol*. 2023;13:1090773. doi:10.3389/fimmu.2022.1090773
55. Scozzi D, Liao F, Krupnick AS, et al. The role of neutrophil extracellular traps in acute lung injury. *Front Immunol*. 2022;13:953195. doi:10.3389/fimmu.2022.953195
56. Ni J, Li G, Dai N, et al. Esculin alleviates LPS-induced acute lung injury via inhibiting neutrophil recruitment and migration. *Int Immunopharmacol*. 2023;119:110177. doi:10.1016/j.intimp.2023.110177
57. Lingaraju A, Long TM, Wang Y, et al. Conceptual barriers to understanding physical barriers. *Semin Cell Dev Biol*. 2015;42:13–21. doi:10.1016/j.semcdb.2015.04.008
58. Major J, Crotta S, Finsterbusch K, et al. Endothelial AHR activity prevents lung barrier disruption in viral infection. *Nature*. 2023;621(7980):813–820. doi:10.1038/s41586-023-06287-y
59. Liu PF, Feng YT, Li HW, et al. Ferrostatin-1 alleviates lipopolysaccharide-induced acute lung injury via inhibiting ferroptosis. *Cell Mol Biol Lett*. 2020;25(1):10. doi:10.1186/s11658-020-00205-0
60. Li XY, Jamal M, Guo PP, et al. Irisin alleviates pulmonary epithelial barrier dysfunction in sepsis-induced acute lung injury via activation of AMPK/SIRT1 pathways. *Biomed Pharmacother*. 2019;118:109363. doi:10.1016/j.biopha.2019.109363
61. Zhao L, Zhang H, Li N, et al. Network pharmacology, a promising approach to reveal the pharmacology mechanism of Chinese medicine formula. *J Ethnopharmacol*. 2023;309:116306. doi:10.1016/j.jep.2023.116306
62. Guo J, Zhang QY, Xu L, et al. Icariin ameliorates LPS-induced acute lung injury in mice via complement C5a-C5aR1 and TLR4 signaling pathways. *Int Immunopharmacol*. 2024;131:111802. doi:10.1016/j.intimp.2024.111802
63. Li N, Cheng Y, Jin T, et al. Kaempferol and ginsenoside Rg1 ameliorate acute hypobaric hypoxia induced lung injury based on network pharmacology analysis. *Toxicol Appl Pharmacol*. 2023;480:116742. doi:10.1016/j.taap.2023.116742
64. Ding Q, Zhu WX, Diao YR, et al. Elucidation of the mechanism of action of ginseng against acute lung injury/acute respiratory distress syndrome by a network pharmacology-based strategy. *Front Pharmacol*. 2021;11:611794. doi:10.3389/fphar.2020.611794
65. Kim KH, Kim JO, Park JY, et al. Antibody-drug conjugate targeting c-kit for the treatment of small cell lung cancer. *Int J Mol Sci*. 2022;23(4):2264. doi:10.3390/ijms23042264